Zone of apposition in the passive diaphragm of the dog

ALADIN M. BORIEK, JOSEPH R. RODARTE, AND SUSAN S. MARGULIES
Department of Medicine, Baylor College of Medicine, Houston, Texas 77030; and Department of Bioengineering, University of Pennsylvania, Philadelphia, Pennsylvania 19104

Boriek, Aladin M., Joseph R. Rodarte, and Susan S. Margulies. Zone of apposition in the passive diaphragm of the dog. *J. Appl. Physiol.* 81(5): 1929–1940, 1996.—We determined the regional area of the diaphragmatic zone of apposition (ZAP) as well as the regional craniocaudal extent of the ZAP (ZAP_{ht}) of the passive diaphragm in six paralyzed anesthetized beagle dogs (8–12 kg) at residual lung volume (RV), functional residual capacity (FRC), FRC + 0.25 and FRC + 0.5 inspiratory capacity, and total lung capacity (TLC) in prone and supine postures. To identify the caudal boundary of the ZAP, 17 lead markers (1 mm) were sutured to the abdominal side of the costal and crural diaphragms around the diaphragm insertion on the chest wall. Two weeks later, the dogs' caudal thoraces were scanned by the use of the dynamic spatial reconstructor (DSR), a prototype fast volumetric X-ray computer tomographic scanner, developed at the Mayo Clinic. The three-dimensional spatial coordinates of the markers were identified (±1.4 mm), and the cranial boundary of the ZAP was determined from 30–40 1.4-mm-thick sagittal and coronal slices in each DSR image. We interpolated the DSR data to find the position of the cranial and caudal boundaries of the ZAP every 5° around the thorax and computed the distribution of regional variation of area of the ZAP and ZAP_{ht} as well as the total area of ZAP. The ZAP_{ht} and area of ZAP increased as lung volume decreased and were largest near the lateral extremes of the rib cage. We measured the surface area of the rib cage cephaled to the ZAP (A_L) in both postures in another six beagle dogs (12–16 kg) of similar stature, scanned previously in the DSR. We estimated the entire rib cage surface area ($A_{rc} = A_{ZAP} + A_L$). The A_{ZAP} as a percentage of A_{rc} increased more than threefold as lung volume decreased from TLC to RV, from ~9 to 29% of A_{rc}.

respiratory muscles; chest wall mechanics; rib cage

THE DIAPHRAGMATIC ZONE OF APPOSITION (ZAP) is defined as the region where the diaphragm is apposed to the rib cage, from the insertion of the diaphragm on the rib cage to the point where the diaphragm begins to peel away from the chest wall. The functional significance of the ZAP as a surface reservoir, i.e., a pathway for change in volume, and as a site of action of abdominal pressure (Pab) on the rib cage has been discussed by Mead (11).

The area of ZAP is crucial in determining the ability of the diaphragm to expand the rib cage. Similowsky et al. (13) showed that in chronic obstructive disease the diaphragm pressure-generating ability was well preserved when adjusted for lung volume. However, with chronic hyperinflation, the decreased area of ZAP reduces the diaphragm's inspiratory action on the rib cage. This inspiratory action may not be sufficient to counteract the decrease in pleural pressure (Ppl) over the surface of the lung, an expiratory effect of the diaphragm that tends to displace the rib cage inward.

Little information is available from direct measurements about the regional variation of area of the ZAP with lung volumes and body posture. In this paper, by the use of the dynamic spatial reconstructor (DSR), we computed the distribution of the regional area as well as regional craniocaudal extent of the ZAP (ZAP_{ht}) at five lung volumes spanning the vital capacity in two body postures in anesthetized paralyzed dogs. The DSR is a fast volumetric X-ray computed-tomographic scanner with high accuracy for longitudinal and volumetric measurements (6). Furthermore, we estimated the total internal surface area of the rib cage ($A_{rc} = A_{ZAP} + A_L$, where A_L is area of the rib cage cephaled to ZAP), as well as the surface area of the portion of the rib cage covered by the ZAP (A_{ZAP}) at functional residual capacity (FRC) and at total lung capacity (TLC).

We use the geometry for the caudal boundary of the ZAP measured in this study, combined with geometry of the lower ribs and costal diaphragmatic muscle fibers measured in our previous studies (see Refs. 10 and 1), to make inferences about the insertional action of the passive diaphragm on the rib cage.

METHODS

Seventeen 1-mm lead markers were sewn to the abdominal surface of the diaphragm around its insertion on the chest wall (see Fig. 1) in six bred-for-research beagle dogs (*group I*, weight 8–12 kg). The dogs were allowed 2–3 wk of postoperative recovery. Each dog was anesthetized, paralyzed, and placed in the posture of interest in the DSR. Previous studies (6) have documented the accuracy of longitudinal and volumetric measurements in the DSR. Lung volume was varied from TLC to residual lung volume (RV) by using a calibrated syringe connected to the endotracheal tube. The inspiratory capacity (IC) was defined as the volume of air required to increase the airway pressure from 0 to 30 cmH_2O. The volume of gas in the lung at 30 cmH_2O was defined as TLC.

The thorax was scanned at five lung volumes spanning the vital capacity: RV, FRC, FRC + 0.25 IC, FRC + 0.5 IC, and TLC, first in the prone and then in the supine position. The three-dimensional rectangular coordinates (X, Y, Z) of the bead positions were determined (±1.4 mm) from the reconstructed DSR images and converted to cylindrical coordinates (R, ω, Z). These points defined the caudal boundary of the ZAP where the diaphragm inserts on the chest wall. The cephalad edge of the ZAP where the diaphragm peels off the chest wall was identified and digitized in 30–40 1.4-mm-thick coronal and sagittal slices spaced 5.6 mm apart. A typical sagittal and coronal slice is shown in Fig. 2, indicating points on the cranial boundary of the ZAP in a supine dog.

We interpolated the DSR data to find the position of the cephalad and caudal boundaries of the ZAP every 5° around the thorax and computed regional ZAP area and regional ZAP_{ht}. The azimuthal position (ω) was defined as 0° at the spine, between 0 and 180° on the right hemidiaphragm, 180° at the sternum, and between 180 and 360° on the left hemidiaphragm of the dog.

Because of scan field limitations, the image data set included only the caudal one-half of the rib cage, thus we

0161-7567/96 $5.00 Copyright © 1996 the American Physiological Society

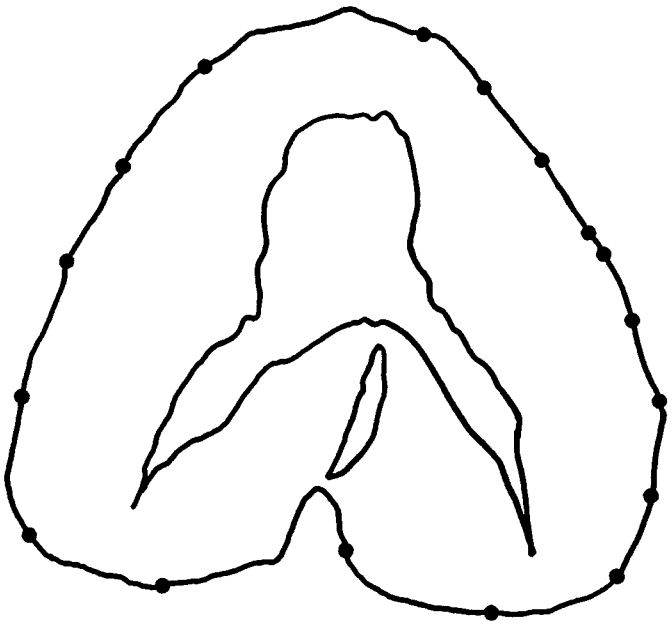

Fig. 1. Schematic of abdominal surface of excised canine diaphragm showing typical location of 17 markers on chest wall insertions. Markers were implanted surgically on the abdomen side of diaphragm around the ring of insertion of diaphragm on the chest wall.

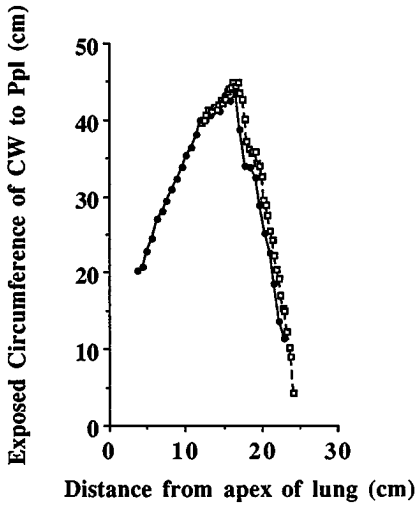

Fig. 3. Circumference of rib cage exposed to pleural pressure (Ppl) plotted against cephalocaudal distance from apex of lung. Dotted line represents diaphragm scans (*group I*). Solid line represents thorax scan (*group II*). CW, chest wall.

could not determine the surface area of the entire thorax in dogs used in the current study (*group I*). In this context, the entire thorax is defined as the thoracic cavity above the caudal boundary of the ZAP of the diaphragm to the chest wall. Previously, the thoraces of another set of beagle dogs (*group II*, weight 12–16 kg) had been scanned in the DSR from the apex to the cephalad boundary of ZAP at the same lung volumes and postures of those of *group I* (10). In both groups, the circumference or curvilinear region of the chest wall exposed to the lung was measured in horizontal slices (*group I*: 1.4 mm thick, spaced 2.8 mm apart; *group II*: 1.6 mm thick, spaced 6.4 mm apart). In general, *group I* rib cage measurements extended from the caudal boundary of the ZAP to the mid-thorax, whereas the *group II* measurements extended from the cephalad boundary of the ZAP to the apex and the arrows of the lung. The rib cage circumference exposed to the lung as a function of the cephalocaudal distance from the apex of the lung for a prone dog at TLC from each group (body weights 11.5 and 12.5 kg, respectively, for *group I* and *group II* dogs) is shown in Fig. 3. There is good agreement between these two groups of animals of similar stature. In fact, across both groups, there was no systematic influence of body weight on the chest wall circumference at the cephalocaudal level of the T_9–T_{10} thoracic vertebral junction, nor was there systematic influence of body weight on the lung-exposed rib cage surface area within each group. The lack of effect of body weight occurred because the dogs were from an inbred strain of laboratory beagles, and most of

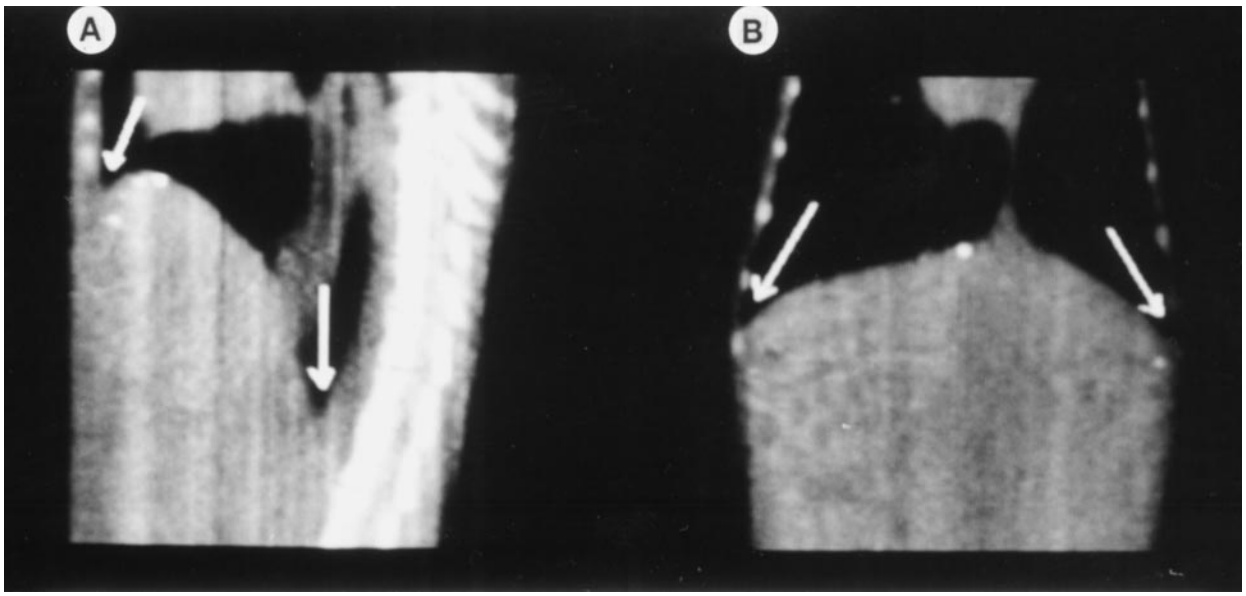

Fig. 2. A typical sagittal (*A*) and coronal (*B*) slice, with arrows indicating *top* of zone of apposition (ZAP). Lead markers appear as bright dots on diaphragm surface. Cephalad edge of ZAP was identified in 30–40 1.4-mm-thick coronal and sagittal slices, spaced 5.6 mm apart.

the difference in body weight occurred because animals housed in the kennel gained weight. The inspiratory capacities of all animals were similar. Thus rib cage circumference data from *groups I* and *II* were combined to determine A_L.

Group I data were used to find the portion of A_L from T_9–T_{10} to ZAP, and *group II* data were used to find A_L from T_9–T_{10} to the apex of the lung. Linear interpolation between digitized slices was used to estimate rib cage circumference for every slice and at the T_9–T_{10} junction. In *group I*, the average lower lung-apposed rib cage surface area was calculated by multiplying slice thickness by circumference and summing from T_9–T_{10} to the base of the lung for each dog, and then averaging across dogs. The same procedure was used in *group II* between T_9–T_{10} and the apex of the lung. These two average values were added together to compute A_L at TLC and FRC in the prone and supine postures. We estimated the entire rib cage area A_{rc} above the diaphragmatic insertion on the chest wall by summing A_L with the average ZAP (*group I* dogs only).

A plane of the form $Ax + By + Cz + D = 0$ was used to fit points on the cranial or points on the caudal boundaries of the ZAP of the left or right hemidiaphragms by minimizing the sums of the squares of the perpendicular distances between the point locations and the plane (1). These planes were fitted to the points on the cranial or caudal boundaries of ZAP at lung volumes varying between RV and TLC. The direction cosines for the normal to the plane *A*, *B*, and *C* were computed by solving the minimization problem

$$\text{minimize } F = \sum_{i=1}^{n} (Ax_i + By_i + Cz_i + D)^2 \qquad (1)$$

subject to the condition

$$A^2 + B^2 + C^2 = 1 \qquad (2)$$

The best fit plane is denoted as the $\eta\zeta$ plane. The coordinates η, ζ, ξ are defined such that the $\eta\zeta$ axes are in the best fit plane of the points on the caudal boundary of the ZAP of the left or right hemidiaphragm, and the axis ξ is in the direction perpendicular to the $\eta\zeta$ plane. The relation of the $\eta\zeta$ plane to the anatomical Cartesian coordinates, the *X*, *Y*, *Z* coordinates, is shown in Fig. 4. The *XZ* plane is sagittal, the *YZ* plane coronal, and the *XY* plane transverse. The *X*-axis is downward, *Z*-axis is headward, and the *Y*-axis is right to left in prone dogs, and left to right in supine dogs. The coordinate η is along the intersection of the sagittal plane and the best fit plane. The coordinate ζ is along the intersection of the coronal plane and the best fit $\eta\zeta$ plane.

The position of the markers of the caudal boundary of the ZAP projected onto a single plane, the $\eta\zeta$ plane, is shown for the left hemidiaphragm in the prone and supine postures in Fig. 4. The angle between the ζ- and *Y*-axes is ϕ. The tilt of the $\eta\zeta$ plane away from the sagittal plane is given by the angle ϕ; when ϕ is 90°, there is no tilt of the $\eta\zeta$ from the sagittal plane. The tilt of the $\eta\zeta$ plane away from a coronal plane is described by ψ, the angle between the η- and the *X*-axes. When ψ is 90°, there is no tilt from the coronal plane; when these angles are zero, the plane is transverse.

The points on the cranial boundary of the ZAP of the left hemidiaphragm were fitted to a plane, $\eta'\zeta'$ plane. The η' coordinate is the intersection between the *XZ* plane and the $\eta'\zeta'$ plane. The ζ' coordinate is the intersection of the $\eta'\zeta'$ plane and the *YZ* plane. The positions of the cranial boundary of the ZAP are described by the angles ϕ' and ψ' that describe the orientation of the $\eta'\zeta'$ plane with respect to the anatomical planes. For example, ϕ' describes the angle between the ζ' and the *Y*-axis, whereas ψ' describes the angle between the η' and the *X* direction.

RESULTS

The orientation of the best fit plane of the markers on the caudal boundary of the ZAP, the $\eta\zeta$ plane, is expressed by the angles ψ and ϕ. The variation of the angles ψ and ϕ with lung volume for each hemidiaphragm was examined by using analysis of variance (ANOVA). In the supine posture, ANOVA indicated that the angles ψ and ϕ are significantly different when the left and right hemidiaphragms are compared ($P < 0.001$). In the prone posture, the angle ϕ was significantly ($P < 0.002$) different between the left and right hemidiaphragms. Lung volume does not affect ψ (supine: $P = 0.12$; prone: $P = 0.94$) or ϕ (supine: $P = 0.09$; prone: $P = 0.93$); see Fig. 5, *A*–*D*. Because lung volume was not a significant influence, the values for ψ and ϕ are averaged over all lung volumes. To facilitate comparisons between the left and right hemidiaphragms, we report the absolute values of ψ and ϕ. In the prone position, the mean angles ±SD across dogs of ψ are 34.4 ± 3.3 and 28.4 ± 8.6° for the left and right hemidiaphragms, respectively. The corresponding values of the angles ϕ are 7.1 ± 5.6 and 18.9 ± 15.6°. In the supine position, the values of ψ are 29.2 ± 3.3 and 26.2 ± 4.9° for the left and right hemidiaphragms, respectively; and the corresponding values of ϕ are 0.6 ± 9.4 and 11.6 ± 9.9°. The $\eta\zeta$ planes of the two hemidiaphragms tilt caudally from a sagittal plane at the midline of the dog to the chest wall and tilt caudally from the sternum to the spine.

The orientation of the best fit plane, the $\eta'\zeta'$ plane, of the cranial boundary of the ZAP is described by the angles ϕ' and ψ'. The mean ± SD values of those angles across dogs, at lung volumes varying between TLC and RV for prone and supine positions, are shown for the left and right hemidiaphragms in Fig. 5, *A*–*D*, respectively. The orientation of the $\eta'\zeta'$ plane is affected by lung volume. The tilt of the $\eta'\zeta'$ plane away from a coronal plane is described by ψ', the angle between the η' and the *X*-axis. This tilt is significantly different among lung volumes ranging from FRC + 0.25IC to RV in prone dogs (5*A*) and between TLC and FRC + 0.25IC for supine dogs (5*B*) (ANOVA; $P < 0.0001$). At low lung volumes prone, when ZAP increases and lung volume decreases, the upper border of ZAP is more closely aligned to the *X*-axis, whereas with inflation above FRC + 0.25IC there is a greater cephalocaudal tilt in the ventrodorsal direction of the upper border of the ZAP, which then remains constant over this volume range. In the supine position, a similar cephalocaudal tilt of the upper border of ZAP in the ventrodorsal direction is observed at TLC, but ψ decreases to ~10° at FRC + 0.5IC and remains essentially constant as ZAP increases from this lung volume to RV. In both postures, the angle ϕ' is independent of lung volume. This indicates that the angle ϕ' is invariant with total area of the ZAP. The tilt of the left hemidiaphragm is significantly different from that of the right hemidia-

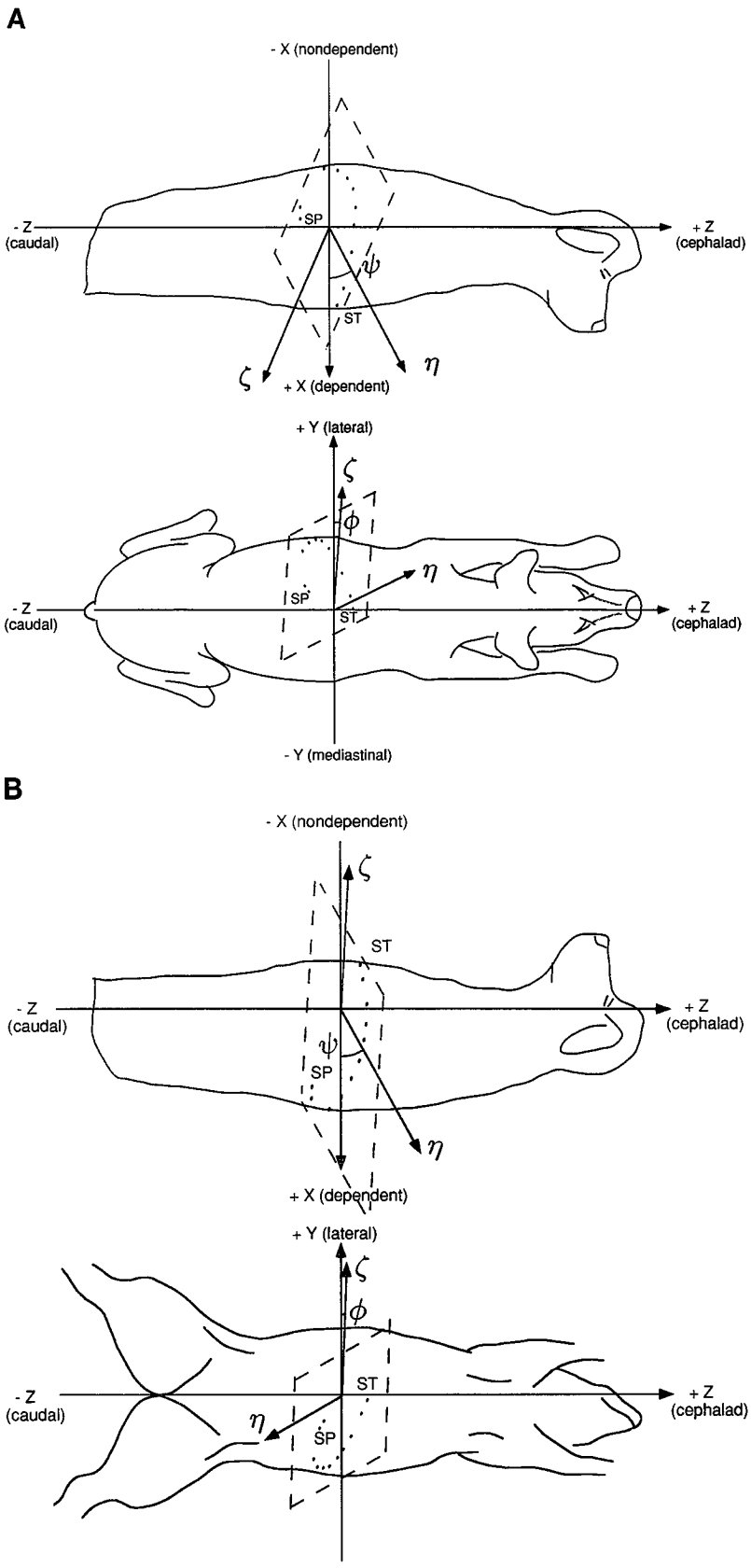

Fig. 4. Location and orientation of caudal boundary of ZAP of left hemidiaphragm in prone position (*A*) and supine position (*B*). *XZ* plane is sagittal with *X*-axis downward and *Z*-axis headward. The η, ζ are such that ηζ axes are in best fit plane of points on the caudal boundary of the insertion on chest wall of the left hemidiaphragm. Its orientation relative to anatomical Cartesian coordinate system (*X*, *Y*, *Z*) is described by the angles ψ and ϕ. Angle ψ is angle between η- and *X*-axes. Angle ϕ is angle between ζ- and *Y*-axes. SP, region near the spine; ST, region near the sternum.

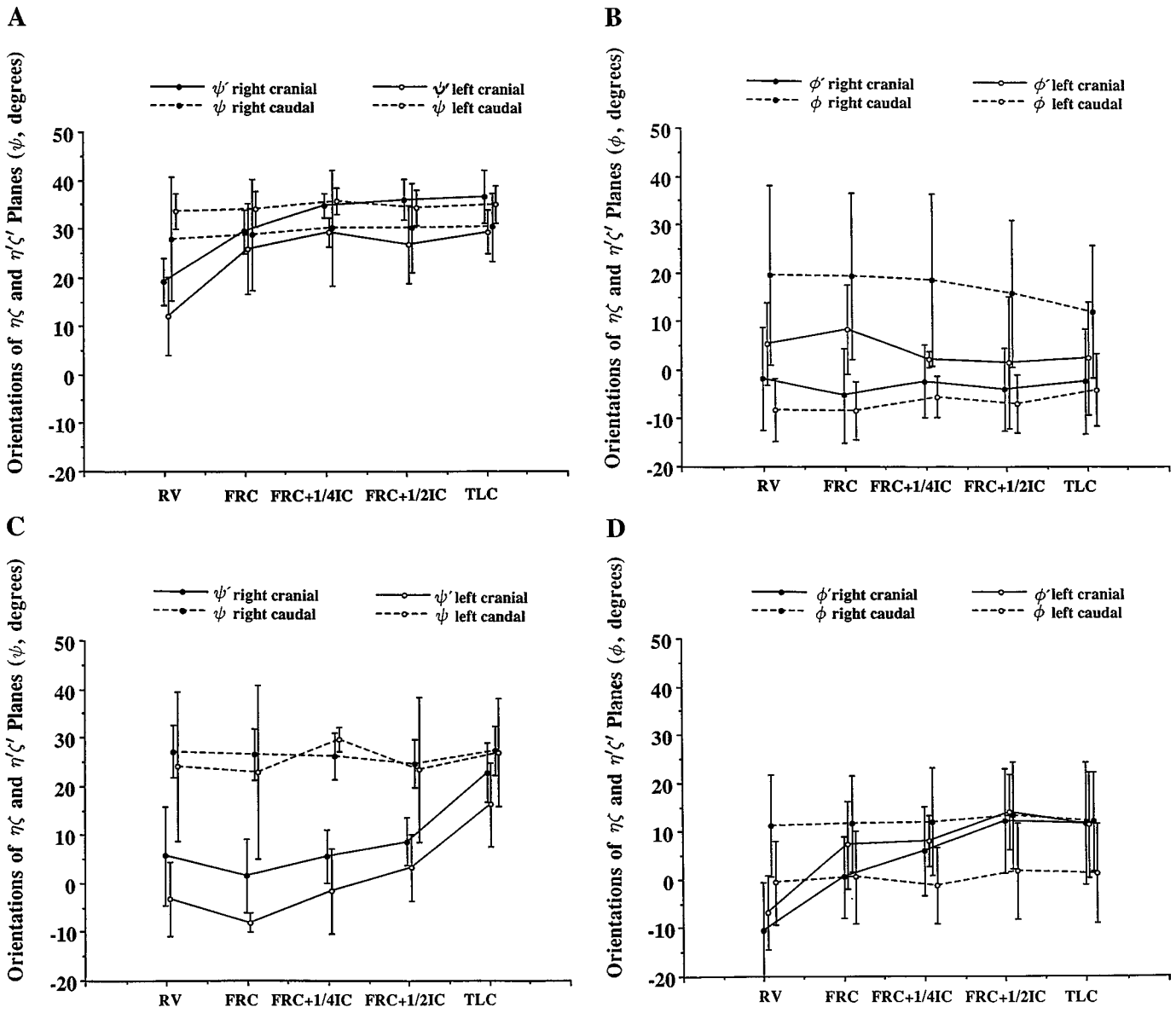

Fig. 5. Means ± SD, across dogs, are shown for angles that describe orientation of best fit planes of caudal and cranial boundaries of ZAP of the left and right hemidiaphragms, at lung volumes varying between total lung capacity (TLC) and lung residual volume (RV) in both prone (*A* and *B*) and supine (*C* and *D*) positions. Angles ψ and ϕ describe orientation of the best fit planes, ηζ, of caudal boundaries of the left and right hemidiaphragms. Angles ψ′ and ϕ′ describe orientation of the best fit planes, η′ζ′, of cranial boundaries of the left and right hemidiaphragms. Changes in lung volume alter orientation of η′ζ′ planes but do not significantly alter orientation of ηζ planes. FRC, functional residual capacity; IC, inspiratory capacity.

phragm in the supine position ($P < 0.0001$) but not significantly different in the prone position.

When the orientations of the ηζ and η′ζ′ planes are compared, in the prone position (Fig. 5, *A* and *B*), for the right hemidiaphragm, the angle ψ′ is significantly greater than ψ at TLC ($P_{TLC} < 0.018$). There is no significant difference between ψ′ and ψ at lung volumes below TLC. However, for the left hemidiaphragm, the angle ψ is significantly greater than the angle ψ′ at lung volumes below FRC + 0.5 IC ($P_{FRC+0.25IC} < 0.028$, $P_{FRC} < 0.048$, $P_{RV} < 0.0004$). The angles ϕ′ and ϕ are not significantly different for either hemidiaphragm across all lung volumes. In the supine position (Fig. 5, *C* and *D*), for the right hemidiaphragm, the angle ψ′ is significantly smaller than ψ at lung volumes below TLC ($P_{FRC+0.5IC} < 0.0006$, $P_{FRC+0.25IC} < 0.002$, $P_{FRC} < 0.001$, $P_{RV} < 0.009$). However, for the left hemidiaphragm, the angle ψ′ is signifciantly smaller than ψ at all lung volumes ($P_{TLC} < 0.023$, $P_{FRC+0.5IC} < 0.007$, $P_{FRC+0.25IC} < 0.001$, $P_{FRC} < 0.009$, $P_{RV} < 0.007$). For the right hemidiaphragm, the angle ϕ′ is significantly smaller than ϕ only at RV ($P_{RV} < 0.005$). In contrast, for the left hemidiaphragm, the angle ϕ′ was significantly different than ϕ at TLC and FRC + 0.25IC ($P_{TLC} < 0.025$, and $P_{FRC+0.5IC} < 0.012$).

The angle $\alpha_{cranialZAP}$ is the angle between the two best fit planes for the two hemidiaphragms at the cranial boundaries of the ZAP. The angle $\alpha_{caudalZAP}$ is the angle

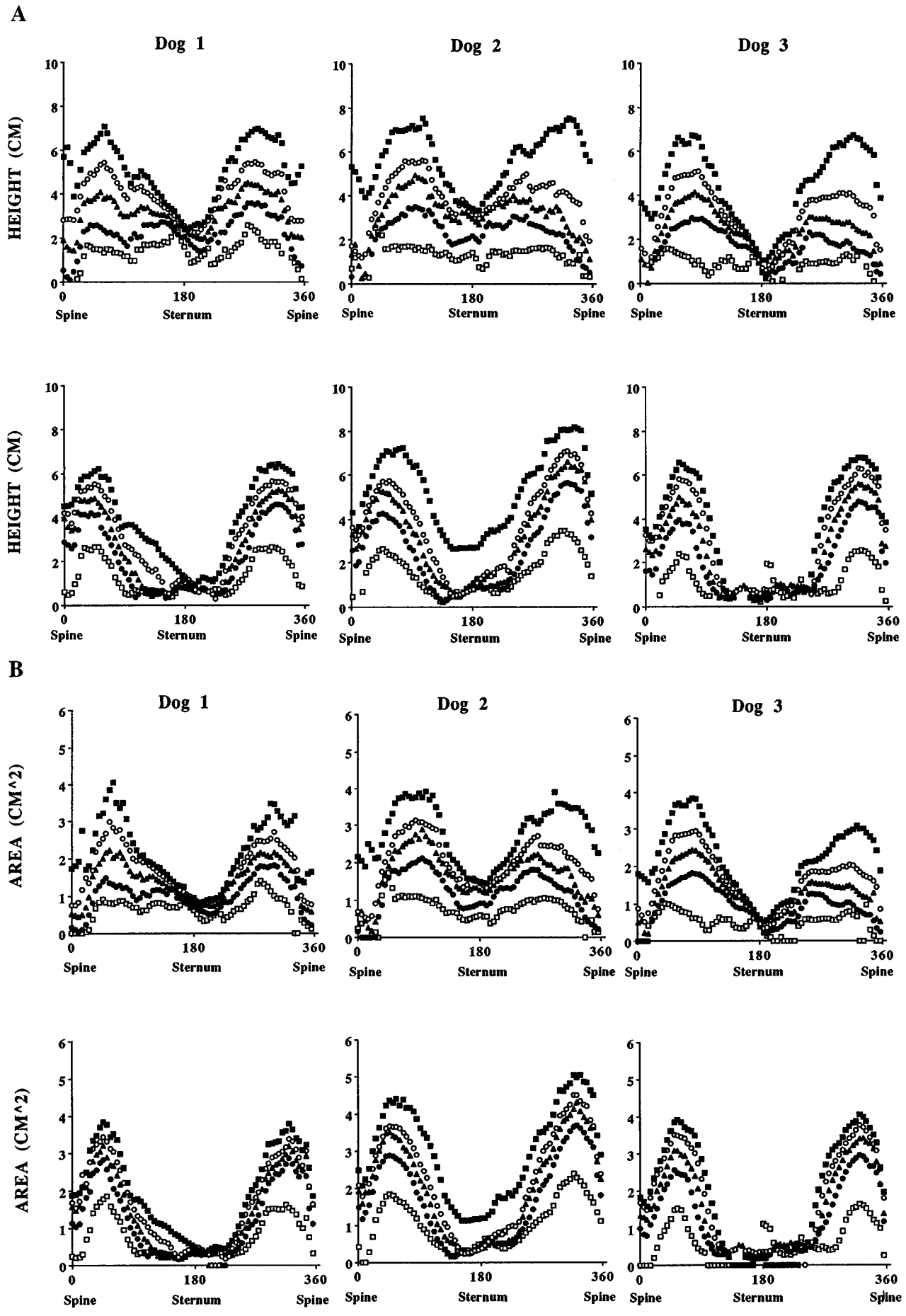
A
Dog 1
Dog 2
Dog 3
HEIGHT (CM)
HEIGHT (CM)
0
2
4
6
8
10
0
180
360
Spine
Sternum
Spine
B
Dog 1
Dog 2
Dog 3
AREA (CM^2)
AREA (CM^2)
0
1
2
3
4
5
6
0
180
360
Spine
Sternum
Spine

between the two best fit planes of the two hemidiaphragms at the caudal boundaries of the ZAP. We computed these angles, $\alpha_{cranialZAP}$ and $\alpha_{caudalZAP}$, and found them to be invariant with lung volume. Their average values ±SD SD in the supine posture were $\alpha_{cranialZAP} = 164.6 \pm 9.9°$ and $\alpha_{caudalZAP} = 157.9 \pm 10.8°$. In the prone posture, these values were $\alpha_{cranialZAP} = 152.7 \pm 13.2°$ and $\alpha_{caudalZAP} = 163.4 \pm 9.2°$.

Distribution of the regional ZAP_{ht} and regional area of the ZAP in three representative prone and supine dogs are shown in Fig. 6, *A* and *B*, respectively, for five different lung volumes ranging from TLC to RV. These results are remarkably similar across dogs. In the ventral region at azimuthal angle of ~180°, the ZAP is smaller when it is gravitationally nondependent in the supine posture than when it is gravitationally dependent in the prone posture.

We computed the azimuthal angle at which the ZAP area was maximum (ω_{maxZAP}) in the left and right hemidiaphragms. To facilitate comparison between the left and right hemidiaphragms, ω_{maxZAP} was measured from the spine. The angle ω_{maxZAP} for the left was significantly different from the right hemidiaphragm in both postures (ANOVA; supine: $P < 0.001$; prone: $P < 0.0019$). The angle ω_{maxZAP} was invariant with lung volume (ANOVA; supine: $P = 0.92$; prone: $P = 0.95$). The mean and ±SD SD of ω_{maxZAP} across dogs in each hemidiaphragm are shown for the prone and supine dogs in Fig. 7. Postural change has significant effect on ω_{maxZAP}. In both hemidiaphragms, the angle ω_{maxZAP} was significantly greater in prone than in supine posture (left: $P < 0.005$; right: $P < 0.05$).

We examined the variation of the area of the ZAP and ZAP_{ht} by using ANOVA. We found a significant effect of lung volume ($P < 0.0001$), posture ($P < 0.007$), and azimuthal position ω ($P < 0.0001$) on the height and area of ZAP. A significant interaction between posture and lung volume ($P < 0.0002$) was found. This interaction may explain the finding that at higher lung volumes, especially at TLC, the height and area of the ZAP at ω_{maxZAP} seemed to be greater in the supine than in the prone position. Because lung volume is constant at TLC, this implies that the distribution of the regional area of the ZAP changes with posture.

The means ±SD SD of the total area of the ZAP for supine and prone postures across dogs are shown in Fig. 8. The area of the ZAP is inversely related to lung volume. The total area of the ZAP increased for prone and supine dogs 3.5 and 3 times, respectively, as lung volumes decreased from TLC to RV. The difference in the change in ZAP area, however, was found to be insignificant between prone and supine positions.

We computed the total area of the lung-apposed portion of the rib cage A_L as well as A_{ZAP} in supine and prone dogs at FRC and at TLC. The total area of the internal surface of rib cage, A_{rc}, expressed in terms of the sum of A_L and A_{ZAP}, is shown in Fig. 9. The A_{rc} increases by ~16% with increasing lung volume from FRC to TLC. Postural changes did not affect the magnitude of the A_{rc}.

The A_{ZAP} as a percentage of the entire rib cage area at a lung volume equal to FRC is shown for prone and supine postures in Fig. 10. The A_{ZAP} increased more than threefold, as lung volume decreased from TLC to RV, from ~9 to 32% of the A_{rc} in the prone posture and from 9 to 26% of the A_{rc} in the supine posture.

DISCUSSION

Mead (11) discussed the importance of the direct inspiratory effects of the insertional force of the diaphragmatic muscle on the rib cage, as well as the effect of transmission of Pab through the ZAP, displacing the rib cage cephalad and outward. The two effects discussed by Mead were implicitly considered axial and radial, respectively. The anatomic data presented here permit a more detailed analysis of these effects. The direction of the insertional force is determined by the orientation of the line of insertion. The force applied by Pab through the ZAP is determined by the distribution of the area of the ZAP. The mechanical effects of these forces are determined by their orientation relative to the rigid ribs of the caudal chest wall.

Fractional muscle shortening (14) and diaphragm displacement (4) differ between spontaneous and mechanical ventilation. If the orientation of the line of insertion and distribution of the area of ZAP was different during active contraction of the diaphragm from that during passive inflation, an analysis of active forces based on anatomy during passive volume changes would be inaccurate. However, displacement of the insertion of the costal diaphragm and its shape during spontaneous and mechanical ventilation were very similar (1), suggesting that error from using passive anatomy to analyze active forces is small.

The resultant force of pressure acting on a closed surface of any shape above a plane is equal to the product of the pressure and the projected area of the surface onto the plane. The resultant of transdiaphragmatic pressure (Pdi) on the left or right hemidiaphragm is a force that is perpendicular to the ηζ plane along the ζ coordinate. If the angle ϕ were zero, bilaterally the right and the left ζ coordinates would both fall in the sagittal plane. However, ϕ is not zero, so that there is small lateral component to the force acting perpendicularly to the ηζ plane. There are two ηζ planes, each fitting the points of insertions of a hemidiaphragm on the chest wall. In addition, there is an angle between the insertional force vectors of the two hemidiaphragms that is equal to α, the angle between the two

Fig. 6. Distribution of regional ZAP_{ht} (*A*) and regional area (*B*) of ZAP in the prone (*top*) and supine (*bottom*) postures of 3 dogs at lung volumes as a function of azimuthal position ω around the thorax. ■, RV; ○, FRC; ▲, FRC + 0.25IC; ●, FRC + 0.5IC; □, TLC in prone and supine postures. ZAP height and area near sternum at an azimuthal angle of 180° was smaller in the supine than in the prone dog. There are no differences in average height or total area of ZAP, due to posture changes.

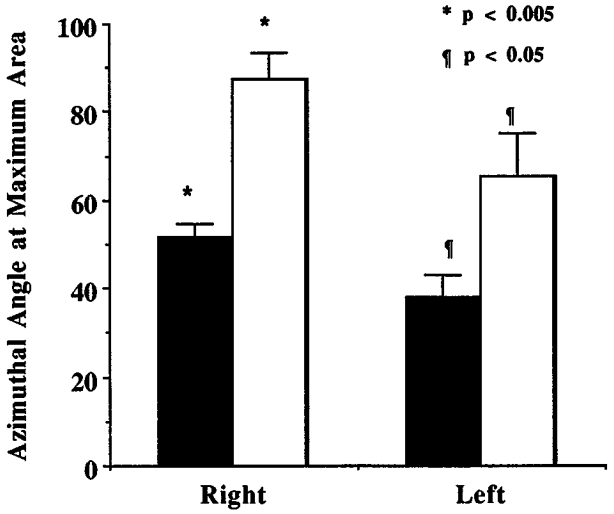

Fig. 7. Average means ± SD across all lung volumes of azimuthal angle ω, at which area of ZAP is maximum (ω_{maxZAP}) for the left and right hemidiaphragms for supine (solid bars) and prone (striped bars) postures. Both values of ω_{maxZAP} for left and right hemidiaphragms were measured from spine. In both hemidiaphragms, angle ω_{maxZAP} is greater in the prone than in the supine position (*left*: $P < 0.05$; *right*: $P < 0.005$).

ηζ planes.The orientation of the ηζ plane to the caudal boundary of the ZAP of either hemidiaphragm in both postures did not change with lung volume. Consequently, the angle between the insertional force vectors of the two hemidiaphragms was invariant with lung volume (prone: 163.4 ± 9.2°, supine: 157.9 ± 10.8°). By using Stokes's theorem (7), the relationship among Pdi, tension (T), and radius of curvature (R) for a uniformly pressurized hemispherical membrane of the diaphragm using the geometry of the insertion planes can be expressed as follows. $Pdi = g(2T/R)$ where g is a geometric parameter (for example, $g = 0.92$ for $\psi = 30°$). The derivation of Stokes's theorem applied to a hemispherical model that inserts on two planes, compared with a model with a single plane of insertion, appears in APPENDIX.

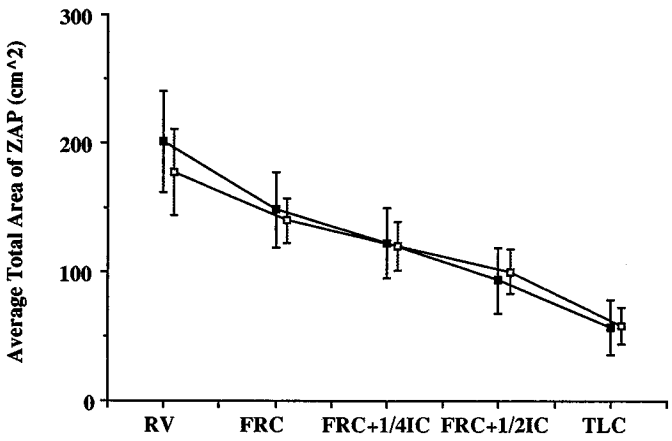

Fig. 8. Total area of ZAP values at RV, FRC, FRC + 0.25IC, FRC + 0.5IC, and TLC, averaged across dogs. Bars represent SD values. Total area increased >3 times as lung volume was decreased from TLC to RV. Changes in total area of apposition due to postural changes were not statistically significant. □, Supine; ■, prone dogs.

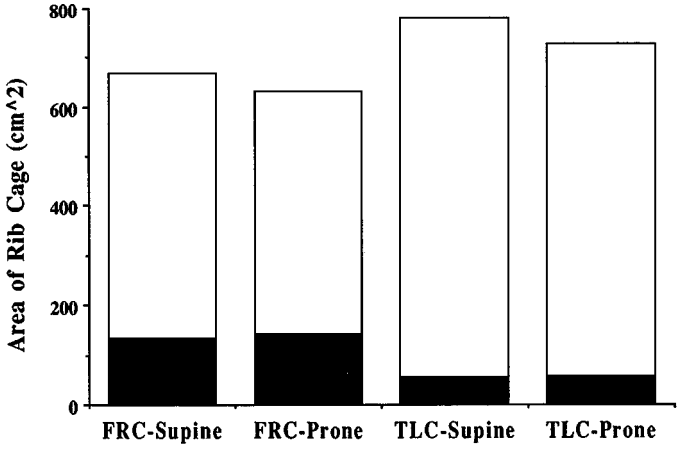

Fig. 9. Total area of the lung-apposed portion (A_L; striped) of rib cage and area of the portion of rib cage covered by ZAP (A_{ZAP}) at TLC and at FRC for supine and prone dogs. Total area of internal surface of the rib cage ($A_L + A_{ZAP}$) appears to be greater at TLC than at FRC. Area of ZAP is greater at FRC than at TLC. Postural changes have no effect on total internal surface area of the rib cage. Solid bars, diaphragm-apposed.

To estimate the angle between the insertional force vectors and the lower ribs, using the anatomical Cartesian coordinate system, we combined *1*) data of Margulies et al. (10) on the orientation of the best fit planes of the lower three ribs of the left side of a beagle dog; *2*) data, computed in our current study, on the orientation of the ηζ plane; and *3*) data, computed from our previous study (1), on the orientation of the plane of a single costal fiber bundle with respect to the left ηζ plane.

We determined the angles between the left ηζ plane computed from the present study and the best fit planes of the sixth, seventh, and eighth ribs, computed from the study by Margulies et al. (10) in the supine posture at FRC. There were no significant differences among the angles between the left ηζ plane and the best fit planes of the lower ribs. Therefore, those angles were averaged across the lower ribs. This means that the

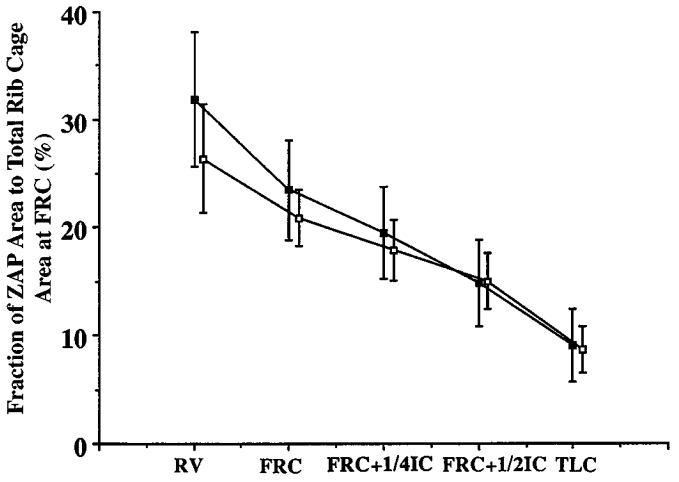

Fig. 10. A_{ZAP} as a percentage of entire rib cage area, computed at a lung volume equal to FRC, is shown for prone (■) and supine (□) postures. A_{ZAP} increased >3 times as lung volume was decreased from TLC to RV.

angle between a lower rib and the line of insertion is ~33°. Because ψ is ~29°, ribs are ~4° from a transverse plane (see Fig. 11).

The mechanical advantage of the insertional force of the diaphragm is dependent on the angle between the force and the ribs. As noted above, there is a lateral component to this force promoting a bucket-handle effect. The pump-handle effect would be maximal if the ribs were parallel to the ring of insertion. Using data from our previous study (1), we computed the average value of the angles of three best fit planes of three muscle fibers, in the midcostal region of the diaphragm, with the best fit plane of the insertional points on the chest wall in supine dogs at FRC. The mean ± SD angle across seven dogs and three muscle fibers was 80.1 ± 2.8°. Therefore, the average angle between the best fit planes of the lower ribs (sixth, seventh, and eighth ribs) and the best fit plane of the muscle fibers in the midcostal region of the diaphragm is ~67° in supine dogs (see Fig. 11). Consequently, the direction of the insertion forces in the midcostal region of the diaphragm is at an angle of ~23° off the direction perpendicular to the plane of a lower rib, indicating that the insertional forces have cephalad and dorsal components.

It is important to distinguish between the insertional forces acting in the perpendicular direction to the ηζ plane and the appositional forces acting in the perpendicular direction to the ηζ plane and the appositional forces acting in the perpendicular direction to the plane of the diaphragmatic ZAP. The insertional forces develop through the insertion of the diaphragmatic muscle fibers into the ribs. The appositional forces, however, are generated by the increase of Pab during the contraction of the diaphragm, which, assuming Pdi is zero, is transmitted across the diaphragm through the ZAP to exert an inspiratory effect on the adjacent inner surface of the rib cage (15, 16). The greater the area of the ZAP, the greater is the inspiratory action of the Pab on the rib cage. Thus the regional distribution of the fraction of the rib cage covered by the ZAP would be an important parameter in determining the distribution of the diaphragmatic appositional force on the rib cage. In addition, the presence of the ZAP ensures that diaphragmatic tension operates on the rib cage through its insertions in a direction that is tangent to the internal surface of the rib cage; thus increasing tension in the diaphragm by these two mechanisms "lifts" the ribs, producing both a pump-handle and a bucket-handle motion of the ribs.

In a previous study, it was demonstrated (1) that the plane of maximum curvature of muscle fibers of the midcostal region of the diaphragm was perpendicular to the line of insertion on the chest wall at FRC, end of inspiration during spontaneous and mechanical ventilation, and at TLC in supine and prone dogs. Given this and the observation that the orientation of the plane of insertions is invariant with respect to lung volume, then the angle between the plane of maximum curvature and the plane of insertions may also be independent of lung volume. The insertional component of the costal diaphragm's inspiratory action on the lower ribs is therefore exerted essentially in the plane of maximum curvature of the costal muscle fibers.

The orientation of the best fit plane to the cranial boundary of the ZAP (η′ζ′ plane) changed with lung volume and posture. The computed angles that describe the orientation of the η′ζ′ plane of the cranial boundary of the ZAP relative to the anatomical Cartesian coordinate system at different lung volumes provided no direct information about the displacement of material points. Nevertheless, the orientation of the η′ζ′ plane provided an insight to diaphragm motion.

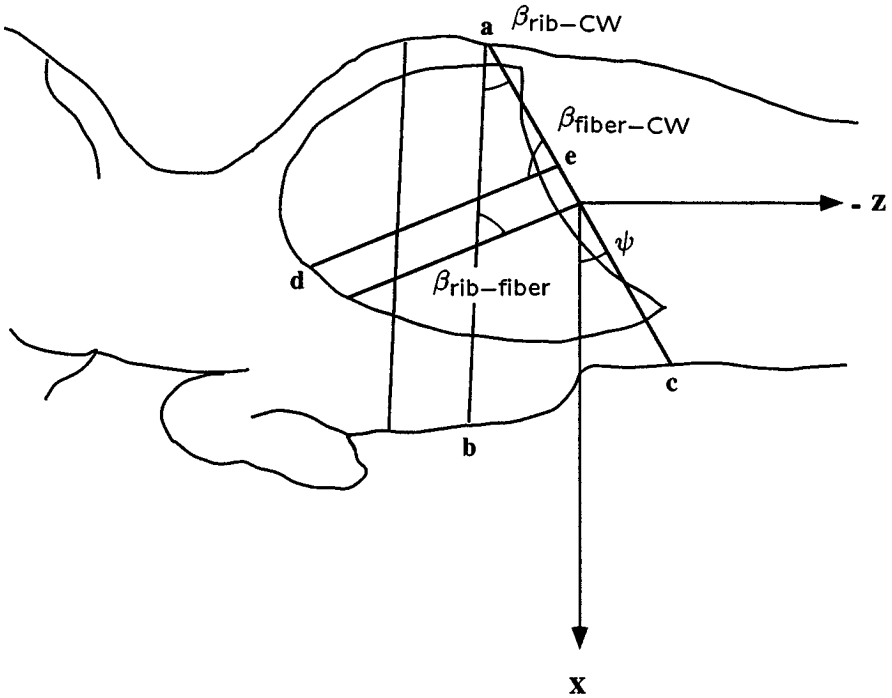

Fig. 11. Schematic representation of a lateral projection image of thorax in a supine dog in anatomical Cartesian coordinate system. *X*-axis is downward, and *Z*-axis is headward. This figure illustrates relationships among orientations of the best fit planes of (*1*) a lower rib (ab), (*2*) caudal boundary of ZAP of left hemidiaphragm (ac), and (*3*) a costal diaphragmatic muscle fiber (de). Angle ψ between insertion line of left hemidiaphragm on the chest wall and the *X*-axis is ~29°. Angle β_{rib-CW}, between a lower rib and insertion line, is ~33°. Angle $\beta_{fiber-CW}$, between muscle fiber and line of insertion, is ~80°. Angle $\beta_{rib-fiber}$, between lower rib and muscle fiber, is ~67°. Lower ribs are ~4° off a coronal plane.

For example, the observation that the orientation of the left $\eta'\zeta'$ plane changes differently with lung volume than does that of the right hemidiaphragm is inconsistent with the pistonlike diaphragm action analogy of Kim et al. (5).

Our results showed that the distributions of the regional area, or the regional ZAP_{ht}, were similar for all lung volumes across dogs. The area of the ZAP decreased with lung volume. At FRC in supine dogs, the fractional area of the internal rib cage surface that constitutes the ZAP was found to be 0.23 ± 0.03%. Macklem et al. (9) estimated the area of the ZAP as a fraction of the total surface area of the rib cage in two supine anesthetized dogs at FRC. The cephalad limit of the ZAP was determined by using two methods: percussion and chest X ray. These values were 0.35 and 0.42%, respectively. It is probable that methodological differences account for differences in results.

The area of the ZAP was smallest at the ventral region in both postures. The ZAP near the ventral surface disappears as the diaphragm peels away from the chest wall with increasing lung volume. This would indicate that the appositional component of the inspiratory force exerted by the diaphragm on the rib cage is smallest in this region. Furthermore, the ventral ZAP was smaller in the supine position when it was gravitationally nondependent than in the prone posture when the ventral ZAP was gravitationally dependent. The maximum area or height of the ZAP occurred near the lateral extremes of the rib cage. The angle ω_{maxZAP} at which maximum area of the ZAP occurred is smaller in the left than that of the right hemidiaphragm. Furthermore, ω_{maxZAP} was greater in the prone than in the supine position. Therefore, the location of maximum appositional component of the inspiratory force of the diaphragm applied to flaring out the lower ribs may be posture dependent. Such a location is more dorsal (gravitationally dependent) in the supine than in the prone position (see Fig. 7).

Mead and Loring (12) estimated that at RV the area of the ZAP in humans occupies nearly one-half of A_{rc} and, therefore, Pab would have a substantial influence on the rib cage. They also proposed that at TLC the ZAP virtually disappears. Our data on dogs showed that the total area of the ZAP increased for prone and supine postures 3.5 and 3 times, respectively, as lung volumes decreased from TLC to RV. Although posture seemed to affect the shape of the ZAP, paired *t*-tests revealed that the posture changes did not influence the total area of the ZAP.

Loring and Mead (8) have suggested a substantial coupling of the rib cage and the abdomen through the ZAP. They developed an analysis of this coupling based on an approximate force balance on the rib cage. The analysis assumes that the rib cage displaces without rotation with a single degree of freedom. Boynton et al. (3) developed a complementary analysis in which mechanical coupling of the rib cage, abdomen, and diaphragm was modeled by a linear translational transformer. Their results were consistent with the findings of Loring and Mead (8) and suggested a substantial pathway coupling. Thus, during diaphragmatic contraction, the reduced Ppl has an expiratory effect on rib cage cephalad of ZAP. The Pab acts to expand the rib cage in ZAP. Thus Pdi (Pdi = Pab − Ppl) tends to distort the rib cage. The inspiratory force on the rib cage acting through ZAP relative to the deflatory force produced by Ppl is given by

$$\frac{\text{Pab}\,\dfrac{A_{ZAP}}{A_{rc}}}{\text{Ppl}\left(1-\dfrac{A_{ZAP}}{A_{rc}}\right)} \qquad (3)$$

Therefore, the ZAP relative to the area of the lung-apposed surface of the rib cage may be an important mechanical parameter that determines the contribution of the Pab to the inspiratory effect on the rib cage.

Using the DSR, Margulies et al. (10) reported data on the orientation and displacements of the ribs at TLC and FRC of anesthetized supine dogs. They demonstrated that rib radii at TLC are uniformly slightly larger than those at FRC, which could only have been caused by a deformation of the costal cartilage. The costal cartilage may become straighter, but it does not stretch, at least not during physiological loads. Therefore, the only way that rib cage area can increase is by increased area between the ribs. We computed the spacing between the ribs in *group II* dogs (12–16 kg) by using data from the study by Margulies et al. (10) at FRC and TLC. We found that spacing between the seventh and eighth ribs for the left side at the lateral extremes was significantly greater ($P < 0.007$) at TLC than those at FRC. The spacing between the ninth and tenth ribs for the right side at the lateral extreme was also found to be significantly greater ($P < 0.027$) at TLC than that at FRC. Therefore, our data that total A_{rc} increased with lung volume as shown in Fig. 8 seem valid. Furthermore, in a previous study (2), the caudal boundary of the ZAP in the midcostal diaphragm demonstrated a slight unexpected caudal displacement with increasing lung volume. Presumably, such a displacement may contribute to the increase of the internal surface of the rib cage shown by the current study. Perhaps most caudal ribs do not follow the cranial displacement of the cranial ribs.

In summary, in the dog, the area of the ZAP between the rib cage and the passive diaphragm increases more than threefold as lung volume decreases from TLC to RV, from ~9 to 29% of the total rib cage area at a lung volume equal to FRC above the origin of the diaphragm. Regional area of ZAP varies around the circumference of the rib cage, and it is largest near the lateral extremes of the rib cage and smallest at the most ventral region, at the sternum. The orientation of the two planes that best fit the caudal boundaries of the ZAP in the two hemidiaphragms is unaffected by lung volume. The orientations of these planes determine the directions of the force vectors of the insertional component of the inspiratory action of the diaphragm on the lower rib cage. The distribution of the regional area of

the ZAP changes somewhat with posture, but total area at a given lung volume is unaffected by postural changes. The regional area of the ZAP determines, in part, the magnitude and distribution of the inspiratory force generated by the apposed diaphragm that expands the dorsal rib cage.

APPENDIX

Using Stokes's theorem (6), we derive of the relationship among pressure, tension, and radius of curvature for two isotropic membrane models subjected to uniform pressure and uniform tension for two models. *Model A*: a hemispherical membrane model simulating the diaphragm with a single boundary plane passing through the points of insertion on the chest wall. These points describe a circle at the base of the hemisphere; and *model B*: a hemispherical membrane model simulating the diaphragm with two boundary planes, the $\eta\zeta$ planes passing through the points of insertion on the chest wall. These points describe two semicircles. An $\eta\zeta$ plane tilts away from a coronal plane by an angle ψ.

Using Stokes's theorem, we derive the relationship among pressure, tension, and radius of curvature for a hemispherical model of the diaphragm with a single plane of insertion on the chest wall (*model A*). A hemispherical membrane surface is defined as $f(x, y, z) = x^2 + y^2 + z^2 = a^2$, where (x, y, z) is the anatomic Cartesian coordinate system and a is the radius of curvature of the hemispherical model. The following is Stokes's theorem (6)

$$\oint_C \vec{\mathbf{T}} \cdot d\vec{\mathbf{R}} = \int\int_S \nabla \times \vec{\mathbf{T}} \cdot \vec{\mathbf{n}} \, d\sigma \qquad (A1)$$

where subscripts C and S are circumference and surface, respectively; $\vec{\mathbf{R}}$ is region bounded by C; $\vec{\mathbf{T}}$ is the tension in the membrane; $\nabla \times \vec{\mathbf{T}} = \vec{\mathbf{P}}$ is the pressure imbalance across the membrane; and $\vec{\mathbf{n}}$ is the surface's unit outward normal vector and is defined as follows

$$\vec{\mathbf{n}} = \frac{x\vec{\mathbf{i}} + y\vec{\mathbf{j}} + z\vec{\mathbf{k}}}{\sqrt{x^2 + y^2 + z^2}} = \frac{x}{a}\vec{\mathbf{i}} + \frac{y}{a}\vec{\mathbf{j}} + \frac{z}{a}\vec{\mathbf{k}}$$

where $\vec{\mathbf{i}}$, $\vec{\mathbf{j}}$, and $\vec{\mathbf{k}}$ are the unit vectors in the coordinate directions. The pressure imbalance across the membrane is defined as $\vec{\mathbf{P}} = P_x\vec{\mathbf{i}} + P_y\vec{\mathbf{j}} + P_z\vec{\mathbf{k}}$.

The following is the right-hand side of Stokes's *Eq. A1*

$$\int\int_S \nabla \times \vec{\mathbf{T}} \cdot \vec{\mathbf{n}} \, d\sigma = \int\int_S \left(P_x \frac{x}{a} + P_y \frac{y}{a} + P_z \frac{z}{a} \right) d\sigma \qquad (A2)$$

The term $d\sigma$ can be defined as follows (6)

$$d\sigma = \frac{|\nabla f|}{|\nabla f \cdot \vec{\mathbf{k}}|} dA, \; |\nabla f| = 2a \text{ and } \nabla f \cdot \vec{\mathbf{k}} = 2z$$

Therefore, $d\sigma = (a/z)dA$. Assume that the pressure imbalance across the membrane is applied along the normal direction $\vec{\mathbf{n}}$, then $\vec{\mathbf{P}} = P\vec{\mathbf{n}}$ and $\nabla \times \vec{\mathbf{T}} \cdot \vec{\mathbf{n}} = P\vec{\mathbf{n}} \cdot \vec{\mathbf{n}} = P$. At the ring of insertion, the normal direction $\vec{\mathbf{n}} = \vec{\mathbf{k}}$ and, therefore, $(P_x, P_y, P_z) = (0, 0, P)$. Now, using *Eq. 2*, we arrive at the following equation

$$\int\int_S \nabla \times \vec{\mathbf{T}} \cdot \vec{\mathbf{n}} \, d\sigma = \int\int_A P \frac{z}{a} \, d\sigma = \int\int_A P \, dA = P\pi a^2 \qquad (A3)$$

Now, consider the left-hand side of Stokes's equation (*A1*). Assume the tension is applied at the insertional points in the perpendicular direction to the plane of insertion. Therefore, $\vec{\mathbf{T}} = T\vec{\mathbf{k}}$. Hence, the following is the left-hand side of Stokes's theorem

$$\oint_C \vec{\mathbf{T}} \cdot d\vec{\mathbf{R}} = T \int_0^{2\pi a} dC = 2\pi a T \qquad (A4)$$

Equating *Eqs. A3* and *A4*, we obtain the following relationship

$$P = \frac{2T}{a} \qquad (A5)$$

Equation A5 describes the relationship among pressure, tension, and radius of curvature for a perfect hemispherical isotropic membrane model of the diaphragm with a single boundary plane of insertions (*model A*).

We now proceed with the derivation for the relationship among pressure, tension, and radius of curvature for *model B* geometry. The tension at the insertion of the hemispherical model of the diaphragm on the chest wall can be defined as follows. Assume that an insertion plane tilts away from a coronal plane by an angle ψ, and using *Eq. A4* we arrive at the following equation

$$\oint_C \vec{\mathbf{T}} \cos\psi \cdot d\vec{\mathbf{R}} = T \cos\psi \int_0^{2\pi a} dC = 2\pi a T \cos\psi \qquad (A6)$$

Define $x^2 + y^2 = a^2$, $x = a\cos\psi$, $y = a\sin\psi$. The following is the right-hand side of Stokes's *Eq. A1*

$$\begin{aligned} \int\int_S \nabla \times \vec{\mathbf{T}} \cdot \vec{\mathbf{n}} \, d\sigma &= \int\int_S P\vec{\mathbf{n}} \cdot \vec{\mathbf{n}} \, d\sigma = P \int\int_S d\sigma \\ &= 4P \int_{x=0}^{a\cos\psi} \int_{y=0}^{\sqrt{a^2 - x^2}} dy \, dx \\ &= 4P \int_0^{a\cos\psi} \sqrt{a^2 - x^2} \, dx \\ &= 4P \int_0^{\sin^{-1}\cos\psi} a^2 \cos^2\psi \, d\psi \\ &= 2Pa^2 \left(\frac{\pi}{2} - \psi + \sin\psi\cos\psi \right) \end{aligned} \qquad (A7)$$

Equating *Eqs. A6* and *A7*, we obtain the following relationship among tension, pressure, and radius of curvature for a perfect hemispherical model of the diaphragm with two planes of insertions

$$\frac{T}{P} = \frac{2a^2 \left(\frac{\pi}{2} - \psi + \sin\psi\cos\psi \right)}{2\pi a \cos\psi}. \qquad (A8)$$

The above equation describes the relationship among membrane tension, pressure imbalance across the membrane, and radius of curvature of the hemispherical model in the case of two boundary planes slanted at an angle ψ to the dorsal ventral direction. Therefore, for *model B* (the angle $\psi > 0$), the pressure imbalance is related to tension and curvature as $P = g(2T/a)$, where g is a geometric factor that depends on the value of the angle ψ. For example, for $\psi = 30$, $g = 0.92$.

The authors thank Daniel Olson for reconstructing the DSR images, and Qing Lin for processing the data. The authors thank the reviewers of this manuscript for their constructive efforts and valuable suggestions.

This work was supported by National Heart, Lung, and Blood Institute research Grants HL-46230, HL-21584, and HL-4664; by the American Lung Association; and by the Whitaker Foundation. The experiments were performed at the Mayo Clinic.

Received March 10, 1995; accepted in final form June 6, 1996.

REFERENCES

1. **Boriek, A. M., S. Liu, and J. R. Rodarte.** Costal diaphragm curvature in the dog. *J. Appl. Physiol.* 75: 527–533, 1993.
2. **Boriek, A. M., T. A. Wilson, and J. R. Rodarte.** Displacement and strains in the costal diaphragm of the dog. *J. Appl. Physiol.* 76: 223–229, 1994.
3. **Boynton, B., G. M. Barnas, J. T. Dadmun, and J. J. Fredberg.** Mechanical coupling of the rib cage, abdomen, and diaphragm through their area of apposition. *J. Appl. Physiol.* 70: 1235–1244, 1991.

3a. **De Troyer, A., M. Sampson, S. Sigrist, and P. T. Macklem.** Action of costal and crural parts of the diaphragm on the rib cage in dog. *J. Appl. Physiol.* 53: 30–39, 1982.

4. **Hubmayr, R. D., and J. R. Rodarte.** Regional ventilation during spontaneous breathing and mechanical ventilation in dogs. *J. Appl. Physiol.* 63: 2467–2475, 1987.
5. **Kim, M. J., W. S. Druz, J. Danon, W. Machnach, and J. T. Sharp.** Mechanics of the canine diaphragm. *J. Appl. Physiol.* 41: 369–382, 1976.
6. **Krayer, S., K. Rehder, K. C. Beck, P. D. Cameron, E. P. Didier, and E. A. Hoffman.** Quantification of thoracic volumes by three-dimensional imaging. *J. Appl. Physiol.* 62: 591–598, 1987.
7. **Kreyszig, E.** *Advanced Engineering Mathematics.* New York: Wiley, 1993.
8. **Loring, S. H., and J. Mead.** Action of the diaphragm on the rib cage inferred from a force-balance analysis. *J. Appl. Physiol.* 53: 756–760, 1982.
9. **Macklem, P. T., D. M. Macklem, and A. De Troyer.** A model of inspiratory muscle mechanics. *J. Appl. Physiol.* 55: 547–557, 1983.
10. **Margulies, S. S., J. R. Rodarte, and E. A. Hoffman.** Geometry and kinematics of dog ribs. *J. Appl. Physiol.* 67: 707–712, 1989.
11. **Mead, J.** Functional significance of the area of apposition of diaphragm to rib cage. *Am. Rev. Respir. Dis.* 119: 31–32, 1979.
12. **Mead, J., and S. H. Loring.** Analysis of volume displacement and length changes of the diaphragm during breathing. *J. Appl. Physiol.* 53: 750–755, 1982.
13. **Similowsky, T., A. P. Gauthier, S. Yan, P. T. Macklem, and F. Bellemare.** Geometry and respiratory displacment of human ribs. *Am. Rev. Respir. Dis.* 147: 850–856, 1993.
14. **Sprung, J., C. Deschamps, R. D. Hubmayr, B. J. Walters, and J. R. Rodarte.** In vivo regional diaphragm function in dogs. *J. Appl. Physiol.* 67: 655–662, 1989.
15. **Urmey, W. F., A. De Troyer, K. B. Kelly, and S. H. Loring.** Pleural pressure increases during inspiration in the zone of apposition of diaphragm to rib cage. *J. Appl. Physiol.* 65: 2207–2212, 1988.